



# Utilization of an energy-resolving detection system for mammography applications: A preliminary study

Eslam M. Taha ,  
Ezzat A. Elmoujarkach ,  
Ahmed Balamesh,  
Samir A. Alzaidi,  
Abdulsalam M. Alhawsawi

**Abstract.** Breast cancer remains one of the major causes of mortality among female cancer patients. This fact caused a spark in the medical field, which in turn helped to improve the diagnostic and treatment of breast cancer patients over the years making this field always active with new ideas and innovative methods. In our study, a new method was explored using an energy-resolving detection system made from a NaI (Tl) scintillation detector to detect the gamma photons from an Am-241 radiation source to try and construct an image by scanning the American College of Radiology (ACR) mammography phantom. In addition to the experimental work, a Geant4 Application for Tomographic Emission (GATE) toolkit was used to investigate more complex options to improve the image quality of mammographic systems, which is limited by the experimental setup. From the experimental setup, the researchers were able to construct an image using the 26.3 keV and the 59.5 keV energy photons, to show the largest size tumour (12 mm) in the ACR phantom. With an improved setup in the simulation environment, the majority of the ACR phantom tumours was visible using both energy windows from the 26.3 keV and the 59.5 keV, where the 26.3 keV yielded better quality images showing four tumours compared to three when using 59.5 keV. The simulation results were promising; however, several improvements need to be incorporated into the experimental work so that the system can generate high-resolution mammographic images similar to the ones obtained by the GATE simulation setup.

**Keywords:** Energy-resolving detection systems • Gamma-ray imaging • GATE simulation toolkit • Mammography

E. M. Taha, A. M. Alhawsawi  
King Abdulaziz University  
Faculty of Engineering, Nuclear Engineering Department  
Jeddah 21589, Saudi Arabia  
and King Abdulaziz University  
Center for Training and Radiation Prevention  
Jeddah 21589, Saudi Arabia

Ezzat A. Elmoujarkach   
King Abdulaziz University  
Faculty of Engineering, Nuclear Engineering Department  
Jeddah 21589, Saudi Arabia  
and Universität zu Lübeck  
Institute of Medical Engineering  
Lübeck, Germany  
E-mail: elmoujarkach@imt.uni-luebeck.de

S. A. Alzaidi  
King Abdulaziz University  
Faculty of Engineering, Nuclear Engineering Department  
Jeddah 21589, Saudi Arabia

A. Balamesh  
King Abdulaziz University  
Electrical and Computer Engineering Department  
Jeddah 21589, Saudi Arabia

Received: 27 September 2021  
Accepted: 3 March 2022

0029-5922 © 2022 The Author(s). Published by the Institute of Nuclear Chemistry and Technology.  
This is an open access article under the CC BY-NC-ND 4.0 licence (<http://creativecommons.org/licenses/by-nc-nd/4.0/>).

## Introduction

Breast cancer remains one of the major causes of death among female cancer patients. It is solely responsible for 15% of all cancer deaths among these patients [1, 2]. The early detection of breast cancer plays a vital role in preventing breast cancer mortality.

Several imaging modalities can be used for breast cancer detection, with each modality having its advantages and disadvantages. However, mammography remains the most popular as it proved to be useful in detection of breast cancer and thereby reducing the mortality [3]. The breast is mainly composed of tissues with similar attenuation properties. The attenuation difference between these tissues is maximum at lower energies. Therefore, mammography uses low-energy X-rays (18–40 kVp) for breast pathology detection. However, the use of low-energy X-rays comes at the expense of a higher radiation dose.

Furthermore, X-rays are produced as a spectrum, where some energies present with no useful information but contribute unnecessarily dose to

the patients. The use of filters helps in reducing the non-useful radiation to a certain level. Scatter radiation also poses an issue in mammography, as it degrades the image contrast. A grid may be used to reduce the scatter radiation but at the expense of increasing the dose to compensate for the primary radiation removed by the grid. Additionally, breast compression is necessary for mammography to reduce breast thickness and consequently scatter radiation and dose [4].

Dose and mortality rate reduction motivated several technological advancements in the field of mammography. The development of digital mammography allowed for higher quality images to be acquired with less dose than screen-film mammography [5, 6]. The advantage of digital tomosynthesis improved the rates of early cancer detection and diagnostic accuracy [7–9].

In recent years,  $\gamma$ -rays have been suggested as an alternative to radiographic X-ray machines. A study of Am-241 feasibility in radiography has been carried out in recent years. In that study, images with acceptable yet inferior quality to X-rays were obtained [10]. In a more recent study, simulations have been carried out suggesting that Am-241 could be a feasible source in mammography applications. The study showed the feasibility of using an energy-resolving detection system to reject photons out of the mammographic energy range [11].

Am-241 emits mainly 59.5 keV photons with a 35.5% yield that is considered beyond the mammographic energy range. The Am-241 also emits 26.3 keV with a 2.4% yield, which is suitable for mammographic usage. Using an energy-resolving detector, as suggested by the study, one can produce acceptable mammographic images and improve contrast significantly through rejection of scattered radiation. These features can be found in pixelated photon-counting detectors.

The use of an energy-resolving photon-counting detector has been utilized extensively in the field of nuclear medicine in gamma cameras and early versions of positron emission tomography (PET) scanners [12, 13].

Green *et al.* [14] obtained scatter-free mammographic images using HEXITEC pixelated spectroscopic detector and reported an improvement of contrast up to 50%. Medipix detectors are another example of photon-counting detectors that showed potential in a wide range of applications [15]. Medipix is a hybrid solid-state pixelated detector that allows the counting of photons of specific energy. Additionally, Medipix can provide coloured, high contrast, and almost noise-free images, allowing for more accurate diagnosis [16–18].

One of the drawbacks of using hybrid solid-state pixelated detectors is that they are thermosensitive, which might require either cooling or operation in a stable low room temperature during imaging [19].

This study aims at exploring the possible advantages of using an energy-resolving detection system with  $\gamma$ -ray radiation sources to produce mammographic images. The system will use a widely available NaI (Tl) scintillation detector that presents

an effective economical solution in obtaining mammographic images at room temperature.

## Materials and methods

### ACR mammography phantom

The ACR mammography phantom is designed to assess the image quality of mammographic systems. The phantom itself contains 16 test objects: six fibers, five microcalcifications clusters, and five masses. The masses have different volumes with a diameter of 12, 9, 7, 5, and 4 mm. For a mammographic system to pass the mammography quality standard act 'MQSA', at least four fibers, three microcalcification clusters, and three masses must be visible [20]. This quality assessment criterion is used to visually evaluate the quality of the images acquired through this study.

### Experimental work

The experimental setup consisted of an Am-241 source, a scanning system, a lead collimator, NaI (Tl) detector, and the ACR mammography phantom. Am-241 is an alpha emitter with a half-life of 432.6 years and emits mainly 59.5 keV (35.9%) and 26.3 (2.3%) [21]. The Am-241 used in this study is housed in a shutter system and has an activity of 1 Ci. The source is cylindrically shaped and has a radius of about 1.5 cm. The experimental setup is shown in Fig. 1.

The ACR phantom is placed in front of the source and held by a mechanical arm. The mechanical arm is controlled by the scanning system. The scanning system specifies the arm movement and the duration of the scan. The arm can be moved vertically or horizontally or in a raster scan.

The collimator is placed on top of the detector to preserve resolution and define the pixel size. It is 2 mm thick and has a 1 mm opening. Smaller openings are possible to fabricate but much more difficult to properly align with the rest of the setup. Additionally, smaller size openings reduce the count rate and therefore increase scanning time. These obstacles are



**Fig. 1.** Experimental setup from left showing the Am-241 in the blue containment shield, the ACR phantom placed in the mechanical arm surrounded with lead blocks to stabilize the arm movement, and finally is the NaI detector with a lead sleeve to shield it from the scattered radiation. 1 – ACR phantom, 2 – NaI crystal, 3 – Am-241 source.

somewhat easier to overcome in simulation; therefore, smaller openings were used in the simulation.

In addition to the collimator, the detector is enclosed within a lead sleeve to prevent scattered photons from reaching the detector's active volume, causing an increase in the dead time.

When the source is turned on, the arm moves the phantom into the first acquisition position. Photons that penetrated the phantom reach the detector collimator. The collimator is aligned with the beam central axis. It blocks radiation outside the field of view from reaching the detector. Detected photons spectroscopic information is processed by the scanning system. After the defined acquisition time elapses, the scanning system stores the spectroscopic data as a function of the acquisition position and moves into the next position. Once the scan is complete, the system uses the acquisition position and spectroscopic information to construct an image, either using the entire spectrum or specific energy channels.

### Simulation

In the simulation, an 11 cm × 11 cm × 4.4 cm phantom with similar characteristics and properties to the ACR mammography phantom was created and the same assessment criteria were used to evaluate the simulated images using Geant4 Application for Tomographic Emission (GATE). GATE is one of the prominent Monte Carlo simulation toolkits with a wide range of applications in the field of medical imaging [22]. The simulation setup consisted of an Am-241 point source, two lead collimators, a NaI detector, and a phantom similar to the ACR mammography phantom as shown in Fig. 2. The number of primers we generated for each energy (59.5 keV and 26.3 keV) was 8 million photons which correspond to the activity of 348 MBq of Am-241. The standard physics processes were enabled in the simulation that included photoelectric effect, Compton scattering, and electron ionization.

The source was placed at a 20 cm distance from the phantom. The emitted radiation is directed toward the phantom as in a cone beam configuration. The beam passes through a 4 mm thick pre-phantom and post-phantom collimators to limit the beam to

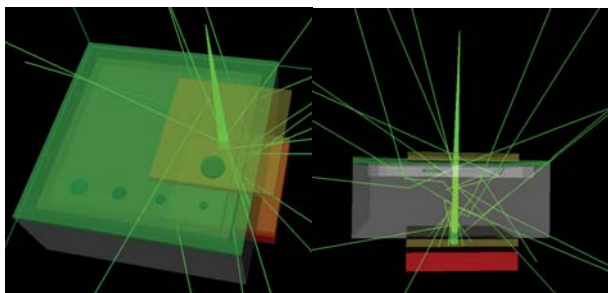


**Fig. 2.** The simulation setup where the green beam represents the  $\gamma$ -rays. The yellow squares are the pre- and post-lead collimators. The red box is the detector. The gray box is the ACR phantom that shows in the top the five masses representing the tumours with diameters of 12, 9, 7, 5, and 4 mm.

the scanned area. The collimator square openings used in the simulation are 0.5 mm and 1 mm, respectively. The post-phantom collimator is placed on top of the NaI detector. The source, detector, and collimators remain stationary all the time while the phantom moves only between acquisitions. The collimator opening size dictates the phantom movement. For a 1 mm opening, the phantom would take a 1-mm horizontal or vertical step between acquisitions. The number of counts for each acquisition is recorded for the 26.3 keV and 59.5 keV windows separately. The acquired data are later used for constructing 2D images using MATLAB.

## Results and discussion

### Experimental work

The source was initially placed at 10 cm from the detector to maximize exposure and reduce the scanning time. Images acquired under this setup exhibited high counting losses due to dead time and pile-up events. As a result, none of the phantom test objects were visible for both energy windows reconstructed images.

To find the optimum distance, two areas in the phantom were imaged at different distances. The first area enclosed the center of the largest tumour. The second enclosed the phantom center (no test object is present in that area). It was evident that the difference in counts between the two points is more distinct at a 35 cm distance. At that distance, scanning the whole phantom would require several hours. Therefore, greater distances were not attempted as it would increase the scanning time further. Very long scanning times caused the system to become unresponsive. Therefore, each phantom object was scanned separately. The acquisition time was set to 150 s/pixel. Reconstructed images for both the 26.3 keV and 59.5 keV windows are illustrated in Fig. 3 for the region containing the largest tumour.

The tumour is visible with both energy windows. However, it is more evident (shows better contrast)

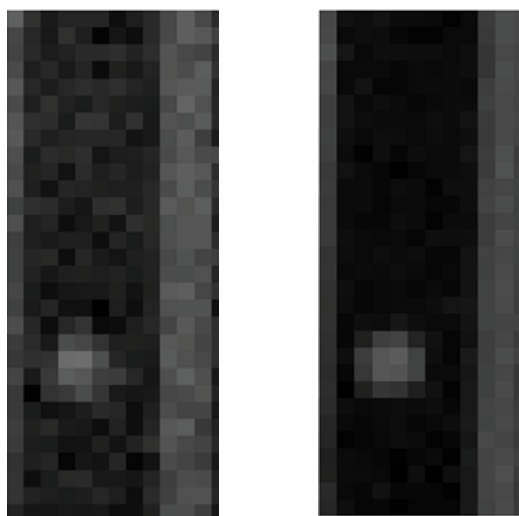


**Fig. 3.** Reconstructed 26.3 keV image (left) and 59.5 keV image (right).



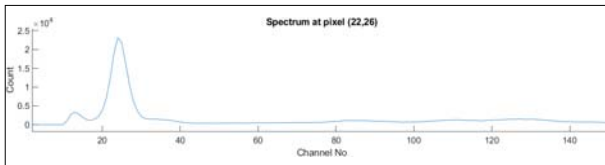


**Fig. 4.** The energy spectrum of a single tumour pixel. The 26.3 keV peak is located at channel 12, while the 59.5 keV peak is located at channel 24.

with the 26.3 keV window, as the attenuation difference between the tumour and normal breast tissue is higher at 26.3 keV. Additionally, 26.3 keV photons have a higher absorption probability in the phantom. As a result, fewer photons reach the detector, and therefore, 59.5 photons produce a higher signal-to-noise ratio image. Figure 4 shows the energy spectrum of a single tumour pixel from both the 26.3 keV and the 59.5 keV.

Typically, the maximum allowed kVp for mammographic X-ray tubes is 40. Higher kVps are not used as the attenuation difference between normal and cancerous cells becomes insignificant beyond 40 keV. Additionally, at higher energies, image contrast deteriorates due to scattered photons becoming the dominant interaction. By eliminating the scattered photons signal component from the image, contrast is expected to improve, and the mammographic energy range could possibly be extended to higher energies.

For comparison, several images were acquired using imaging detectors widely used clinically, such as computed radiography (CR) and flat panel. These detectors are pixelated and therefore, the setup was static during acquisition. The exposure time was set initially to 150 s and was increased gradually up to two days. Additionally, a 1-mm collimator was attached to the source opening to reduced geometrical blurring. However, none of the ACR mammography phantom test objects were detected in all images obtained with the flat-panel and CR detectors. Figure 5 shows a sample image obtained with a 70-micron pixel size computed radiography detector and a 2-day exposure. The incapability of commonly used imaging detectors to detect the largest tumour, even with much higher resolution than our scanning system, distinguishes energy-resolving detectors over other currently clinically employed imaging detectors. Some of the test objects, such as the microcalcifications, have higher attenuation

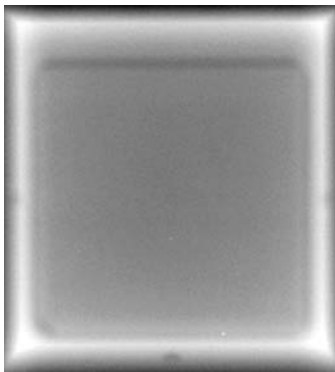


**Fig. 5.** An image of the ACR mammographic phantom taken with Am-241 photons and a computed radiography detector.

differences than tumours with normal tissue. However, they are much smaller in size. Therefore, they are expected to be detected with an energy-resolving detector with a resolution higher than the one employed in this study.

The undetectability of test objects at higher energies shows a distinctive advantage of the energy-resolving detector over other commonly used imaging detectors. Considering the relatively poor resolution of the NaI scanning system, even with relatively poor resolution, it was capable of detecting one of the test objects.

## Simulation

The ideal setup alignment and the absence of signal losses resulted in simulated images having better quality than the experimental ones. Figure 6 illustrates images produced with a 1 mm step. At least three tumours were visible with 26.3 keV photons and two tumours with 59.5 keV photons.

The 59.5 keV images were produced by irradiating the phantom with 22 MBq of Am-241 (8 MBq of 59.5 keV photons). 26.3 keV photons images, on the other hand, were produced with 348 MBq of Am-241, where 8 MBq of these photons are 26.3 keV. Increasing the activity reduces the image noise but does not increase the number of visible objects. Improving the resolution by using 0.5 mm steps increases the number of visible objects for both energy windows, as illustrated in Fig. 7. Fibers show similar behaviour to the tumours as they have similar attenuation coefficients. Three out of six fibers are detected with both energy windows, with the fourth fiber being partially detected. The fourth fiber is very narrow in size and most of its pixels are shared with the background. As a result, its signal is reduced by the averaging effect.



**Fig. 6.** Images produced with 59.5 keV photons (left) and 26.3 keV photons (right) using 1 mm openings.

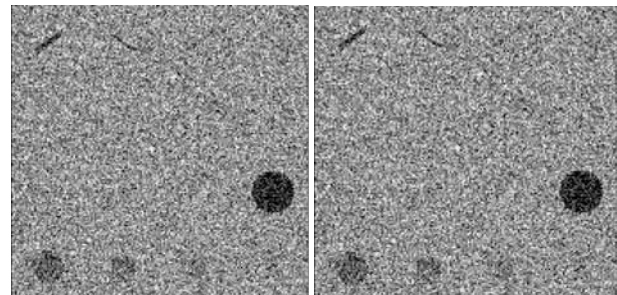


**Fig. 7.** Images produced with 59.5 keV photons (left) and 26.4 keV photons (right) using a 0.5 mm openings.

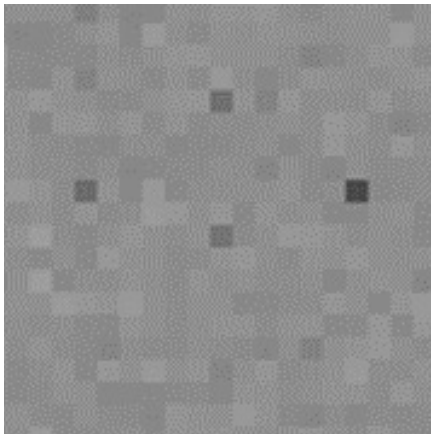


**Fig. 8.** A magnified image of the largest microcalcification cluster. Only four out of six microcalcifications are detected.

Tumours are easier to detect, with the used imaging setup, as they occupy larger areas. On the other hand, microcalcifications are the smallest in size; therefore, more difficult to detect. A single group of microcalcification can be partially detected for both energy windows with 0.5 mm openings, as illustrated in Fig. 8.

The detected cluster only occupies four pixels with each pixel embodying a single microcalcification. Although microcalcifications are the smallest in size, they have the largest attenuation difference with the phantom background. This means that they are typically easier to detect if the imaging system has enough resolution; therefore, more microcalcification can be detected if smaller steps were used.


## Conclusion


The use of an energy-resolving detection system showed a promising result when paired with a gamma source, which can be used for mammogram imaging. A flat panel detector system when used to detect tumours did not show any of the tumors in the ACR mammography phantom as compared to the energy-resolving detection system. A NaI (Tl) scintillation detector was used to reconstruct the objects in the ACR mammography phantom to produce an image. Utilizing simulations, the researchers were able to show the potential images that can be obtained from the ACR mammography phantom with the proposed energy-resolving detection system compared to the experimental work. The research team was also able to present the different images that can be obtained from two different energy windows. To reach the same image quality produced in the simulation environment, several elements in the experimental setup need to be changed and improved such as the size of the collimator, the step size of the mechanical arm, and the source activity.


**Acknowledgment.** This work was funded by the National Plan for Science, Technology and Innovation (MAARIFAH), King Abdulaziz City for Science and Technology, Kingdom of Saudi Arabia (Award No.

10-ELE1077-03). The authors also acknowledge and thank Science and Technology Unit, King Abdulaziz University for their technical support.

## ORCID

A. M. Alhawsawi  <http://orcid.org/0000-0002-7992-8850>

E. A. Elmoujarkach  <http://orcid.org/0000-0003-2750-5984>

E. M. Taha  <http://orcid.org/0000-0002-1867-4703>

## References

1. Ferlay, J., Soerjomataram, I., Dikshit, R., Eser, S., Mathers, C., Rebelo, M., Parkin, D. M., Forman, D., & Bray, F. (2015). Cancer incidence and mortality worldwide: Sources, methods and major patterns in GLOBOCAN 2012. *Int. J. Cancer*, *136*(5), E359–E386. DOI: 10.1002/ijc.29210.
2. Siegel, R. L., Miller, K. D., & Jemal, A. (2018). Cancer statistics. *CA Cancer J. Clin.*, *68*, 7–30.
3. Brem, R. F., Petrovitch, I., Rapelyea, J. A., Young, H., Teal, C., & Kelly, T. (2007). Breast-specific gamma imaging with <sup>99m</sup>Tc-Sestamibi and magnetic resonance imaging in the diagnosis of breast cancer – a comparative study. *Breast J.*, *13*(5), 465–469. DOI: 10.1111/j.1524-4741.2007.00466.x.
4. Bushberg, J. T., Seibert, J. A., Leidholdt, E. M. Jr., Boone, J. M., & Goldschmidt, E. J. (2003). The essential physics of medical imaging. *Med. Phys.*, *30*, 1936.
5. Lewin, J. M., D’Orsi, C. J., Hendrick, R. E., Moss, L. J., Isaacs, P. K., Karellas, A., & Cutter, G. R. (2002). Clinical comparison of full-field digital mammography and screen-film mammography for detection of breast cancer. *Am. J. Roentgenol.*, *179*(3), 671–677. DOI: 10.2214/ajr.179.3.1790671.
6. Obenauer, S., Luftner-Nagel, S., von Heyden, D., Munzel, U., Baum, F., & Grabbe, E. (2002). Screen film vs full-field digital mammography: image quality, detectability and characterization of lesions. *Eur. Radiol.*, *12*(7), 1697–1702. DOI: 10.1007/s00330-001-1269-y.
7. Niklason, L. T., Christian, B. T., Niklason, L. E., Kopans, D. B., Castleberry, D. E., Opsahl-Ong, B. H., Landberg, C. E., Slanetz, P. J., Giardino, A. A., Moore, R., Albagli, D., DeJule, M. C., Fitzgerald, P. F., Fobare, D. F., Giambattista, B. W., Kwasnick, R. F., Liu, J., Lubowski, S. J., Possin, G. E., Richotte, J. F., Wei, C. Y., & Wirth, R. F. (1997). Digital tomosynthesis in breast imaging. *Radiology*, *205*(2), 399–406. DOI: 10.1148/radiology.205.2.9356620.
8. Skaane, P., Bandos, A. I., Gullien, R., Eben, E. B., Ekseth, U., Haakenaasen, U., Izadi, M., Jepsen, I. N., Jahr, G., Krager, M., Niklason, L. T., Hofvind, S., & Gur, D. (2013). Comparison of digital mammography alone and digital mammography plus tomosynthesis in a population-based screening program. *Radiology*, *267*(1), 47–56. DOI: 10.1148/radiol.12121373.
9. Rafferty, E. A., Park, J. M., Philpotts, L. E., Poplack, S. P., Sumkin, J. H., Halpern, E. F., & Niklason, L. T. (2013). Assessing radiologist performance using combined digital mammography and breast tomosynthesis compared with digital mammography alone: Results

- of a multicenter, multireader trial. *Radiology*, 266(1), 104–113. DOI: 10.1148/radiol.12120674.
10. Alyassin, A. M., Maqsood, H. A., Mashat, A. M., Al-Mohr, A. -S., & Abdulwajid, S. (2013). Feasibility study of gamma-ray medical radiography. *Appl. Radiat. Isot.*, 72, 16–29. DOI: 10.1016/j.apraiso.2012.11.001.
  11. Taha, E. E. M., & Alyassin, A. M. A. (2016). Feasibility of a novel gamma radiography mammo system. *Insights Med. Phys.*, 1, 1–8.
  12. Wagenaar, D. J., Chowdhury, S., Engdahl, J. C., & Burckhardt, D. D. (2003). Planar image quality comparison between a CdZnTe prototype and a standard NaI(Tl) gamma camera. *Nucl. Instrum. Methods Phys. Res. Sect. A-Accel. Spectrom. Detect. Assoc. Equip.*, 505(1/2), 586–589. DOI: 10.1016/S0168-9002(03)01153-7.
  13. Taillefer, R. (2021). Scintillation cameras: A new clinical era has come. *J. Nucl. Cardiol.* DOI: 10.1007/s12350-021-02660-4.
  14. Green, F. H., Veale, M. C., Wilson, M. D., Seller, P., Scuffham, J., & Pani, S. (2016). Scatter free imaging for the improvement of breast cancer detection in mammography. *Phys. Med. Biol.*, 61(20), 7246–7262. DOI: 10.1088/0031-9155/61/20/7246.
  15. Russo, P. (2002). Hybrid semiconductor pixel detectors for low- and medium-energy X- and gamma-ray single photon imaging using the Medipix Read-Out Chip. In J. P. Hornak (Ed.), *Encyclopedia of imaging science and technology*. New York: John Wiley & Sons, Inc.
  16. Pfeiffer, K. -F. G., Giersch, J., & Anton, G. (2004). How good is better? A comparison between the Medipix1 and the Medipix2 chip using mammographic phantoms. *Nucl. Instrum. Methods Phys. Res. Sect. A-Accel. Spectrom. Detect. Assoc. Equip.*, 531(1/2), 246–250. DOI: 10.1016/j.nima.2004.06.012.
  17. Manuilskiy, A., Norlin, B., Nilsson, H. -E., & Fröjd, C. (2004). Spectroscopy applications for the Medipix photon counting X-ray system. *Nucl. Instrum. Methods Phys. Res. Sect. A-Accel. Spectrom. Detect. Assoc. Equip.*, 531(1/2), 251–257. DOI: 10.1016/j.nima.2004.06.013.
  18. Procz, S., Lubke, J., Zwerger, A., & Fauler, A. (2010). Energy selective X-ray imaging with Medipix. In IEEE Nuclear Science Symposium & Medical Imaging Conference 2010, pp. 3846–3851. DOI: 10.1109/NSSMIC.2010.5874533.
  19. Yang, Q., Wang, X., Kuang, Z., Zhang, Ch., Yang, Y., & Du, J. (2021). Evaluation of two SiPM arrays for depth-encoding PET detectors based on dual-ended readout. *IEEE Trans. Radiat. Plasma Med. Sci.*, 5(3), 315–321. DOI: 10.1109/TRPMS.2020.3008710.
  20. McLelland, R., Hendrick, R. E., Zinnering, M. D., & Wilcox, P. A. (1991). The American College of Radiology Mammography Accreditation Program. *Am. J. Roentgenol.*, 157(3), 473–479. DOI: 10.2214/ajr.157.3.1872231.
  21. Basunia, M. S. (2006). Nuclear Data Sheets for A = 237. *Nucl. Data Sheets*, 107, 2323–2422.
  22. Jan, S., Santin, G., Strul, D., Staelens, S., Assie, K., Autret, D., Avner, S., Barbier, R., Bardies, M., Bloomfield, P. M., Brasse, D., Breton, V., Bruyndonckx, P., Buvat, I., Chatziioannou, A. F., Choi, Y., Chung, Y. H., Comtat, C., Donnarieix, D., Ferrer, L., Glick, S. J., Groiselle, C. J., Guez, D., Honore, P. -F., Kerhoas-Cavata, S., Kirov, A. S., Kohli, V., Koole, M., Krieguer, M., van der Laan, D. J., Lamare, F., Llargeron, G., Lartizien, C., Lazaro, D., Maas, M. C., Maigne, L., Mayet, F., Melot, F., Merheb, C., Pennacchio, E., Perez, J., Pietrzyk, U., Rannou, F. R., Rey, M., Schaart, D. R., Schmidlein, C. R., Simon, L., Song, T. Y., Vieira, J. -M., Visvikis, D., Van de Walle, R., Wieers, E., & Morel, C. (2004). GATE -Geant4 application for tomographic emission: a simulation toolkit for PET and SPECT. *Phys. Med. Biol.*, 49(19), 4543–4561.